

Article

Protonation Dependent Topological Dichotomy of Core modified Hexaphyrins: Synthesis, Characterization and Excited State Dynamics

Abhijit Mallick, Juwon Oh, Marcin A. Majewski, Marcin St#pie#, Dongho Kim, and Harapriya Rath

J. Org. Chem., **Just Accepted Manuscript** • Publication Date (Web): 15 Dec 2016

Downloaded from <http://pubs.acs.org> on December 16, 2016

Just Accepted

“Just Accepted” manuscripts have been peer-reviewed and accepted for publication. They are posted online prior to technical editing, formatting for publication and author proofing. The American Chemical Society provides “Just Accepted” as a free service to the research community to expedite the dissemination of scientific material as soon as possible after acceptance. “Just Accepted” manuscripts appear in full in PDF format accompanied by an HTML abstract. “Just Accepted” manuscripts have been fully peer reviewed, but should not be considered the official version of record. They are accessible to all readers and citable by the Digital Object Identifier (DOI®). “Just Accepted” is an optional service offered to authors. Therefore, the “Just Accepted” Web site may not include all articles that will be published in the journal. After a manuscript is technically edited and formatted, it will be removed from the “Just Accepted” Web site and published as an ASAP article. Note that technical editing may introduce minor changes to the manuscript text and/or graphics which could affect content, and all legal disclaimers and ethical guidelines that apply to the journal pertain. ACS cannot be held responsible for errors or consequences arising from the use of information contained in these “Just Accepted” manuscripts.

1
2
3
4 Protonation Dependent Topological Dichotomy of
5
6
7
8
9 Core Modified Hexaphyrins: Synthesis,
10
11
12
13
14
15
16
17
18
19
20
21
22
23
24
25
26
27
28
29
30
31
32
33
34
35
36
37
38
39
40
41
42
43
44

Characterization and Excited State Dynamics

Abhijit Mallick,^{†a} Juwon Oh,^{‡a} Marcin A. Majewski,[§] Marcin Stępień,^{§*} Dongho Kim^{‡*} and Harapriya Rath^{†*}

[†] Department of Inorganic Chemistry, Indian Association for the Cultivation of Science, 2A/2B Raja S. C. Mullick Road, Jadavpur, Kolkata 700032(India)

[‡] Department of Chemistry, Yonsei University, Seodaemun-gu, Seoul 120-749 (Korea)

[§] Wydział Chemii, Uniwersytet Wrocławski, ul. F. Joliot-Curie 14, 50-383 Wrocław, Poland

^a Contributed equally

ichr@iacs.res.in

dongho@yonsei.ac.kr

marcin.stepien@chem.uni.wroc.pl

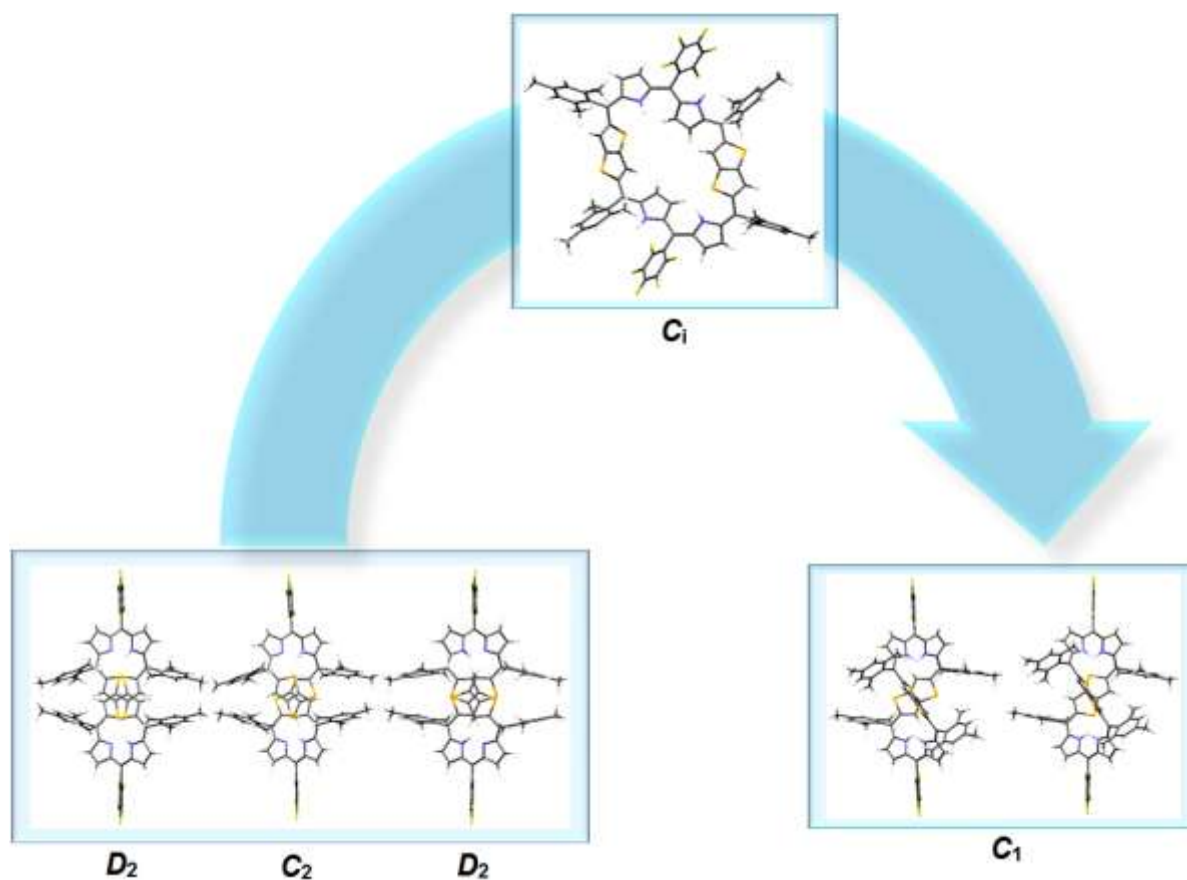
ABSTRACT

45
46
47
48
49
50 Two hitherto unknown core modified hexaphyrin analogues have been synthesized and
51
52 characterized where the conformational dynamics of these macrocycles in the free base form
53
54 is achieved by the rotation of thienothiophene units. Further unique property of these
55
56 macrocycles is the Hückel-Möbius topological switching. The thermodynamic equilibrium
57
58 and kinetics of the interconversion leading to Hückel-Möbius switches has been triggered by
59
60 external stimuli such as protonation and/or temperature. We have provided a thorough

1
2
3
4
5
6
7
8
9
10
11
12
13
14
15
16
17
18
19
20
21
22
23
24
25
26
27
28
29
30
31
32
33
34
35
36
37
38
39
40
41
42
43
44
45
46
47
48
49
50
51
52
53
54
55
56
57
58
59
60

solution-state spectroscopic characterization, solid-state structural evidence combined with in-depth theoretical calculations to investigate the crucial factors involved in such interconversion between Hückel and Möbius topologies for these hexaphyrins which will be useful in designing future new members to expanded porphyrin chemistry.

TOC GRAPHIC



INTRODUCTION

The rational design and synthesis of discrete and pre-organized molecular systems with defined topology¹ are of interest due to their ion binding properties and conformational flexibility and allows one to explore uncharted frontiers in chemistry, biology and other related areas. Recent years have witnessed a renaissance of interest from synthetic chemists

1
2
3 in arriving at structurally nontrivial aromatic molecules with nonorientable (Möbius-band) π
4 surfaces.^{2e} The molecular-orbital description of Möbius aromaticity predicts that singlet
5
6 annulenes with $4n\pi$ electrons are aromatic systems in twisted conformations (with an odd
7
8 number of half-twists) where the p orbitals lie on the surface of a Möbius strip, whereas
9
10 singlet $[4n+2]$ Möbius molecules would be antiaromatic (the opposite of the Hückel rule).²
11
12 Porphyrins and expanded porphyrins serve as a benchmark for extreme manifestations of
13
14 aromaticity, antiaromaticity, pseudo aromaticity, and Möbius aromaticity.³ Because of their
15
16 large conformational flexibility, expanded porphyrins are the best platforms to adopt a
17
18 Möbius topology since the large strain induced by the molecular twist is dissipated across the
19
20 whole macrocyclic ring system. Thus the initial finding of a Möbius porphyrinoid, A,D-di-*p*-
21
22 benziporphyrin,^{4a} was followed by subsequent reports on other Möbius aromatic
23
24 porphyrinoids containing $[24]\pi$ or larger electronic conjugation pathways, which were
25
26 stabilized and controlled by various factors, such as metal coordination, temperature, solvent
27
28 effects, protonation equilibria, and peripheral substitution.⁴ Much progress has been made in
29
30 these endeavors but much remains unexplored. Hence there is an upsurge in demand for new
31
32 synthetic expanded porphyrins for an in-depth study of aromaticity and π -conjugation. From
33
34 literature reports, it is inferable that in sharp contrast to topographically flat fully conjugated
35
36 expanded porphyrins, the propensity of figure-eight twisted geometries towards
37
38 conformational fluxionality leads to topological switching from one conformation to another
39
40 depending upon the protonation state and metallation.^{5,6a} So far, multi-level switching
41
42 behavior in a single macrocyclic entity has not been reported in all-pyrrole expanded
43
44 porphyrins^{4g} and their heterologues containing O, S, Se or Te.^{4h, 4i, 6a} Experimental
45
46 realization of new conformationally flexible expanded porphyrins might provide model
47
48 systems for investigating the key issue of topologically controlled aromaticity switching.
49
50
51
52
53
54
55
56
57
58
59
60

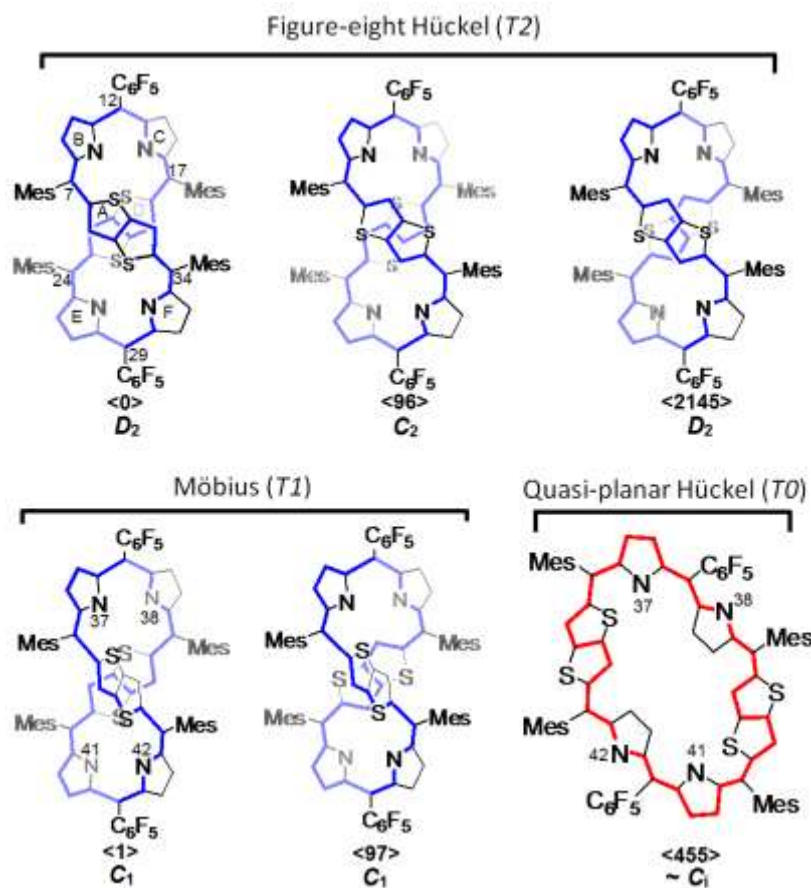
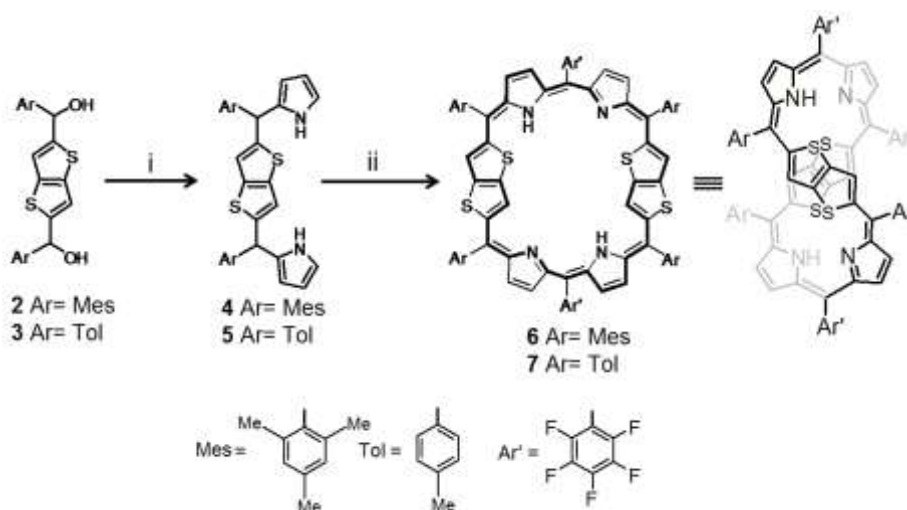


Chart 1. Conformations of **6-H₂** and **7-H₂** discussed in the paper. π -conjugation and NH protons pattern are not shown for clarity

RESULTS AND DISCUSSION

Here we report the successful synthesis of two $[32]\pi$ heteroannulenes **6-H₂** and **7-H₂** (Scheme 1). These systems are (1.1.1.1.1.1) hexaphyrin analogues containing two thieno[3,2-*b*]thiophene subunits (henceforth designated as TT) and six *meso* bridges,⁶ and differ in their *meso* substituents adjacent to the TT units (tolyl vs. mesityl). The above design was chosen with the aim of creating conformationally flexible systems that might exhibit three distinct π -conjugation topologies depending upon the external stimuli. In an initial step leading to target macrocycles, thieno[3,2-*b*]thiophene **1** was synthesized following a literature report.⁷

Because the steric bulk of the *meso*-aryl substituents play a decisive influence on the efficiency of macrocyclization,⁸ two different tripyrrane analogues **4** and **5** were synthesized in two steps from **1** (Scheme S1).⁹ The rational synthesis of macrocycles **6-H₂** and **7-H₂** entailed a mild protic acid-catalyzed condensation of either **4** or **5** with pentafluorobenzaldehyde followed by oxidation with chloranil under reflux.⁶ The addition of 0.1 equivalent of *p*-toluene sulfonic acid gave the best yield for macrocycles **6-H₂** and **7-H₂**. Column chromatographic separation over basic alumina followed by repeated silica gel (200-400 mesh) chromatographic separation yielded the macrocycles **6-H₂** and **7-H₂** in 6% and 8% yields, respectively, as dark green solids.



Scheme 1. Synthesis of macrocycles **6-H₂**, **7-H₂**. Reagents and conditions: i) pyrrole (50 equiv), trifluoro acetic acid (1 equiv); ii) pentafluorobenzaldehyde, cat. PTSA, chloranil (2.5 equiv)

The new macrocycles were thoroughly characterized via spectroscopic and single crystal X-ray diffraction analyses. Macrocycles **6-H₂** and **7-H₂** showed the parent ion peaks at m/z 1416.464 and 1304.156 respectively, under positive ionization in MALDI-TOF mass spectrometry (Figure S6, S7), thus confirming their elemental composition.

1
2
3 The expanded macrocycles **6-H₂** and **7-H₂** were anticipated to show considerable
4 conformational flexibility, as previously observed for various expanded porphyrinoids.^{4, 5, 6}
5
6 In both molecules, the structure bears a formal resemblance to A, D-di-*p*-benzihexaphyrin,^{4a,}
7
8 ^b because of the presence of two quasi-linear subunits (TT vs. *p*-phenylene) in the macrocycle.
9
10 On the basis of this similarity, a range of conformers were considered for the present ring
11 systems, to facilitate further analysis. The lower symmetry of the rotatable TT fragments
12 produces a larger number of distinct conformations that need to be considered, and we found
13 it advantageous to classify these structures using the previously reported binary system.^{3e} In
14 particular, there are three distinct arrangements of the TT units in the figure-eight Hückel
15 structure (denoted *T2*, because of the corresponding linking number $Lk = 2$).^{3e,4c} In these
16 arrangements, labeled $\langle 0 \rangle$, $\langle 96 \rangle$, and $\langle 2145 \rangle$ in Chart 1, the non-hydrogen atom framework can
17 have the limiting point symmetry D_2 , C_2 and D_2 , respectively. Likewise two distinct Möbius
18 *T1* structures, $\langle 1 \rangle$ and $\langle 97 \rangle$, each of C_1 symmetry, can be considered. The symmetry of these
19 conformations can be further lowered by protonation. In parallel with the spectroscopic work,
20 we used DFT calculations to systematically analyze the geometries and relative energies for
21 different protonation states of the above skeletal structures. Relevant results of this analysis
22 are discussed below (for complete computational data, see the Supporting information).
23
24
25
26
27
28
29
30
31
32
33
34
35
36
37
38
39
40
41
42

43 We have carried out thorough NMR studies in the free base as well as in the protonated
44 state in order to investigate the relationship between solution-state dynamic conformational
45 changes and aromaticity in **6-H₂** and **7-H₂**. Dynamic NMR studies support the premise that
46 depending on the relative orientation of TT units at the crossing point, there are two *T2* type
47 conformers in the free base form of the macrocycle **6-H₂** (Chart 1). The temperature-
48 dependent behavior of the ¹H NMR spectra of free base **6-H₂** in CD₂Cl₂ indicates an effective
49 D_2 symmetry, which is inferred from the equivalence of all mesityl groups and the non-
50 equivalence of mesityl *o*-Me signals. This symmetry is consistent with a figure-eight Hückel
51
52
53
54
55
56
57
58
59
60

1
2
3 structure that does not untwist on the NMR time scale, while undergoing a rapid NH proton
4 transfer even at 175 K (Figure 1). Below 250 K, decoalescence of the peak at 18.12 ppm
5 takes place, indicating two forms with different populations (the peaks at 17.75 and 18.61
6 ppm for major and minor species, respectively). The population of minor form decreases
7 upon decreasing temperature (from 0.20 at 220 K to 0.15 at 175 K). The ^1H NMR spectrum
8 of the major conformer is similar to that at high-temperature spectrum and only a very weak
9 ROE is observed between NH and TT protons at 190 K, representing the D_2 symmetry
10 (Figure S30). These features are consistent with the orientation of TT units found in the $\langle 0 \rangle$
11 conformation of **6**-H₂ (Chart 1). This assignment is further supported by DFT calculations,
12 which predict the lowest energy for the 37,41H- $\langle 0 \rangle$ -**6**-H₂ structure (Figure 2, Table 1). In the
13 spectrum of the minor conformer, the peaks at 18.61 ppm (NH) and 9.96 ppm (TT) have
14 equal integral intensities and show a strong dipolar contact in the ROESY spectrum (Figure
15 S30). These features correspond to the C_2 -symmetrical conformer $\langle 96 \rangle$, in which one of the
16 TT subunits is rotated by 180° relative to its position in the $\langle 0 \rangle$ structure (Figure 2). The
17 remaining signals of $\langle 96 \rangle$ -**6**-H₂ were difficult to assign because of extensive overlap with the
18 spectrum of major conformer (in particular, the other TT signal of $\langle 96 \rangle$ -**6**-H₂ overlaps
19 precisely with the TT line of $\langle 0 \rangle$ -**6**-H₂). In accord with the experiment, DFT calculations
20 predict 38,42H- $\langle 96 \rangle$ -**6**-H₂ as the second most stable structure (relative ΔG^0_{298} of 0.36
21 kcal/mol, Table 1).
22
23
24
25
26
27
28
29
30
31
32
33
34
35
36
37
38
39
40
41
42
43
44
45
46
47
48

49 The T_2 topology of the π system in the $\langle 0 \rangle$ -**6**-H₂ and $\langle 96 \rangle$ -**6**-H₂ conformers corresponds to
50 two half-twists and an orientable surface. For a [32]annulenoid circuit, this topology is
51 expected to produce a Hückel-antiaromatic $4n\pi$ system. The ^1H chemical shifts are indicative
52 of a moderate paratropic ring current. At 190 K in DCM- d_2 , the paratropicity is demonstrated
53 by the low-field positions of the inner NHs (17.76 and 18.60 ppm for $\langle 0 \rangle$ -**6**-H₂ and $\langle 96 \rangle$ -**6**-H₂),
54 and of the unique TT proton of $\langle 96 \rangle$ -**6**-H₂ residing in the cavity (9.96 ppm). Outer protons
55
56
57
58
59
60

attached to the macrocycle are moderately affected by the ring current effect (β -CHs in the 5.8–6.2 ppm range). Finally in the Mes substituents, the endo *o*-Me groups (3.27 ppm in $\langle 0 \rangle$ -6-H₂) are deshielded relative to those in 5-mesityldipyrin (2.10 ppm), a feature previously shown to indicate paratropicity.^{4b}

Name ^[a]	Topology and protonation	SCF $E^{[b]}$ a.u.	$E_{rel}^{[c]}$ kcal/mol	ZPV ^[d] a.u.	min. freq. ^[e] cm ⁻¹	$\Delta G^{[f]}$ a.u.	$\Delta G_{rel}^{[g]}$ kcal/mol
Neutral							
f_0000_37_41x	37,41H- $\langle 0 \rangle$	-5959.772214	0.00	1.240085	10.48	-5958.668453	0.00
f_0000_37_42	37,42H- $\langle 0 \rangle$	-5959.755199	10.68	1.239838	10.24	-5958.648461	12.55
f_0001_37_41	37,41H- $\langle 1 \rangle$	-5959.757331	9.34	1.240305	8.31	-5958.655465	8.15
f_0001_38_41	38,41H- $\langle 0 \rangle$	-5959.750163	13.84	1.240189	6.72	-5958.650246	11.43
f_0096_37_41a	37,41H- $\langle 96 \rangle$	-5959.769891	1.46	1.239991	10.60	-5958.666208	1.41
f_0096_37_42	37,42H- $\langle 96 \rangle$	-5959.753658	11.64	1.240012	8.84	-5958.648597	12.46
f_0096_38_41	38,41H- $\langle 96 \rangle$	-5959.757720	9.09	1.240223	9.86	-5958.651024	10.94
f_0096_38_42a	38,42H- $\langle 96 \rangle$	-5959.769882	1.46	1.239894	7.42	-5958.667879	0.36
f_0097_37_41	37,41H- $\langle 97 \rangle$	-5959.754737	10.97	1.240038	3.49	-5958.654846	8.54
f_0097_37_42	37,42H- $\langle 97 \rangle$	-5959.757553	9.20	1.240140	7.21	-5958.656100	7.75
f_0097_38_41	38,41H- $\langle 97 \rangle$	-5959.753262	11.89	1.240297	7.39	-5958.653315	9.50
f_0097_38_42	38,42H- $\langle 97 \rangle$	-5959.757536	9.21	1.240427	7.86	-5958.655437	8.17
f_2145_37_41a	37,41H- $\langle 2145 \rangle$	-5959.767270	3.10	1.239846	10.26	-5958.665594	1.79
f_2145_37_42	37,42H- $\langle 2145 \rangle$	-5959.753887	11.50	1.239799	5.80	-5958.651880	10.40
Monocations							
f_0000	37,38,41H- $\langle 0 \rangle$	-5960.217048	0.00	1.254180	9.54	-5959.096765	1.07
f_0001_37_38_41	37,38,41H- $\langle 1 \rangle$	-5960.204840	7.66	1.254197	7.96	-5959.088483	6.26
f_0001_37_38_42	37,38,42H- $\langle 1 \rangle$	-5960.210743	3.96	1.254142	8.88	-5959.094168	2.70
f_0001_37_41_42	37,41,42H- $\langle 1 \rangle$	-5960.207898	5.74	1.254125	7.86	-5959.091944	4.09
f_0001_38_41_42	38,41,42H- $\langle 1 \rangle$	-5960.205744	7.09	1.254662	7.13	-5959.088943	5.97
f_0096_37_38_41	37,38,41H- $\langle 96 \rangle$	-5960.216025	0.64	1.254055	10.39	-5959.098015	0.28
f_0096_37_38_42	37,38,42H- $\langle 96 \rangle$	-5960.214118	1.84	1.253815	9.61	-5959.096644	1.14
f_0097_37_38_41	37,38,41H- $\langle 97 \rangle$	-5960.207275	6.13	1.254465	7.53	-5959.090403	5.06
f_0097_37_38_42	37,38,42H- $\langle 97 \rangle$	-5960.211155	3.70	1.254076	8.20	-5959.095982	1.56
f_0097_37_41_42	37,41,42H- $\langle 97 \rangle$	-5960.208800	5.18	1.253957	7.70	-5959.093433	3.16
f_0097_38_41_42	38,41,42H- $\langle 97 \rangle$	-5960.207787	5.81	1.254977	7.52	-5959.091205	4.55
f_2145	37,38,41H- $\langle 2145 \rangle$	-5960.212983	2.55	1.254012	8.82	-5959.098463	0.00
Dications							
f_0000a	37,38,41,42H- $\langle 0 \rangle$	-5960.648235	1.00	1.268539	7.85	-5959.514542	1.30
f_0001	- $\langle 1 \rangle$	-5960.648777	0.66	1.268982	7.80	-5959.516470	0.09
f_0096a	- $\langle 96 \rangle$	-5960.623683	16.41	1.268563	10.86	-5959.485483	19.53
f_0097	- $\langle 97 \rangle$	-5960.649831	0.00	1.269557	7.74	-5959.516608	0.00
f_0455	- $\langle 455 \rangle$	-5960.647519	1.45	1.269560	8.58	-5959.514093	1.58
f_2145	- $\langle 2145 \rangle$	-5960.645949	2.44	1.268316	6.82	-5959.515649	0.60

Table 1. Computational data for 6-H₂ and its cations.

[a] Dataset name (.pdb files). [b] PCM(DCM)/KMLYP/6-31G(d,p) energies for optimized geometries. [c] Relative energies (separately for each protonation level). [d] Zero-point vibrational energy. [e] lowest vibrational frequency. [f] Gibbs free energy. [g] Relative Gibbs free energies (separately for each protonation level).

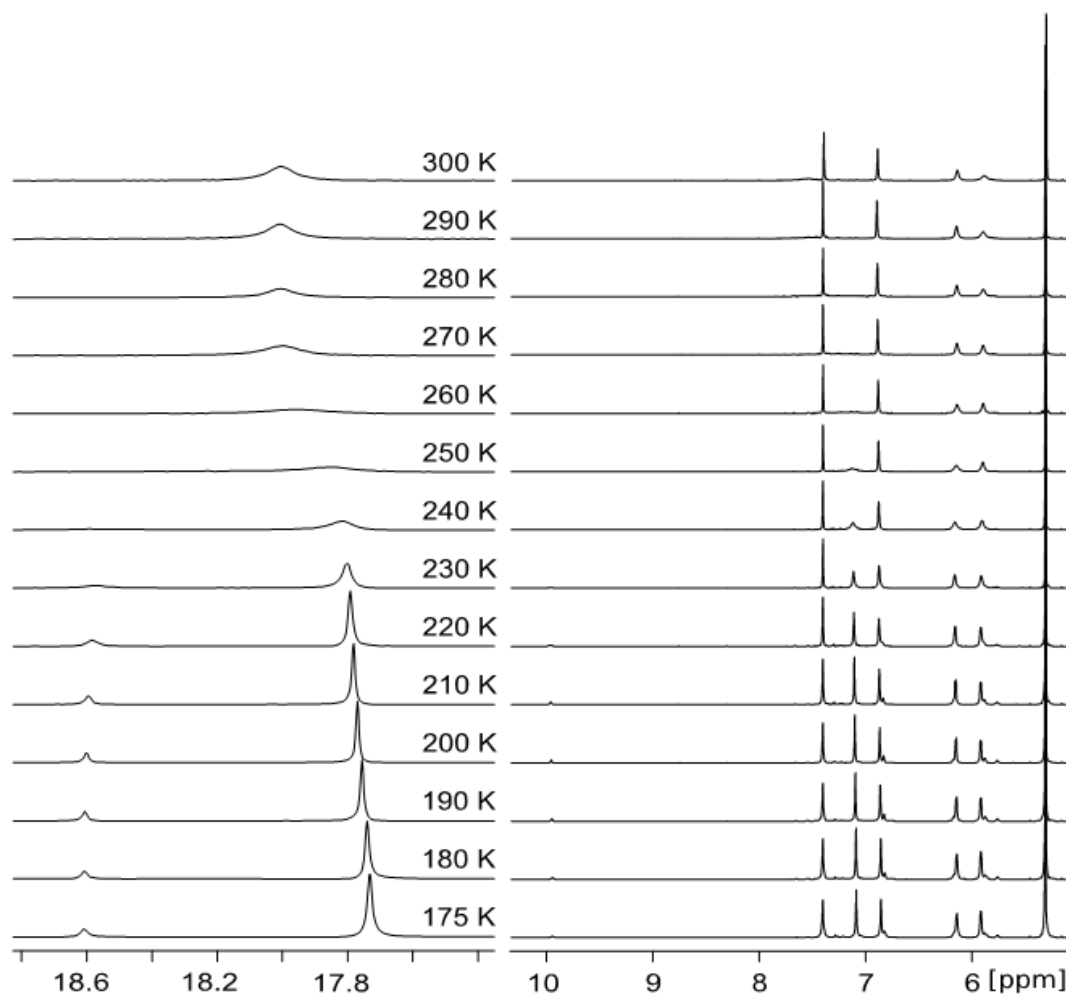


Figure 1. Selected regions of variable temperature ^1H NMR spectra of **6**-H₂ (CD₂Cl₂, 600 MHz)

Importantly, the chemical shift pattern observed for the major form is in good quantitative agreement with GIAO shieldings calculated for the DFT model of 37,41H-⟨0⟩-**6**-H₂ at the KMLYP/6-31G(d,p) level of theory (Figure S31). In the present work, it was not possible to provide complete signal assignment for all species. The completeness of the assignment was limited in several cases by signal overlap and line broadening.

Variable-temperature ^1H NMR measurements performed for **7**-H₂ revealed a similar conformational exchange between the ⟨0⟩ and ⟨96⟩ structures with moderate paratropic ring current. However, at room temperature, single *o*-Tol and *m*-Tol signals were observed,

1
2
3
4 corresponding to rapid exchange between the endo and exo positions in the Tol substituents
5 (Figures S32, S33). This effect could be caused either by rapid rotation of the Tol groups or
6 by inversion of the figure-eight twist of the macrocycle. The former explanation is in line
7
8 with the reduced steric hindrance of the Tol groups in **7-H₂**. As the rigidity of the macrocycle
9
10 should not be significantly affected by the difference of substituents, the barrier to inversion
11
12 is expected to be similar in **6-H₂** and **7-H₂**.
13
14
15
16

17
18 Single crystals suitable for X-ray diffraction were obtained by slow diffusion of
19
20 methanol into toluene solutions of **6-H₂** and **7-H₂**. In the free-base form, macrocycles **6-H₂**
21
22 and **7-H₂** (Figures 3a and S58) were each observed to adopt the twisted Hückel ⟨0⟩
23
24 conformation prevalent in solution. In the structure of **6-H₂**, the dihedral angle for pyrrolic
25
26 ring is 32.66°, for pyrrolic ring is 24.57° and for thienothiophene moiety is 11.24° with
27
28 respect to the mean plane containing the six *meso* carbons. The distance between the
29
30 centroids of the TT units in **6-H₂** and **7-H₂** were 3.80 Å and 3.78 Å respectively.
31
32
33

34
35 The acid-base chemistry of **6-H₂** and **7-H₂** was initially investigated using
36
37 spectrophotometric titrations with trifluoroacetic acid (TFAH) performed in 1, 2-
38
39 dichloroethane (DCE, Figure 4). The free base forms of **6-H₂** and **7-H₂** showed major
40
41 absorption bands at 320, 517 and 658 nm for **6-H₂** and at 357, 511 and 683 nm for **7-H₂**,
42
43 respectively, with absorption tailing over 1400 nm. The latter feature is characteristic of
44
45 antiaromatic porphyrinoids, in line with the observation of *T2*-type conformers by ¹H NMR
46
47 spectroscopy. Both compounds turned out to be relatively weak bases and required a large
48
49 excess of acid to undergo protonation. For each species, two well-defined protonation-related
50
51 events with two isosbestic points were observed (Figure 4). For **6-H₂**, the two stepwise
52
53 spectral changes exhibit isosbestic points at 547 and 617 nm whereas for **7-H₂**, the two
54
55 isosbestic points at 543 and 612 nm respectively upon the two stepwise spectral changes. In
56
57
58 the first event, occurring at ca. 20 equiv of TFAH, a species with a broad, strongly NIR-
59
60

1
2
3 shifted Q-like band was observed, with a maximum at 1500 nm and 1700 nm for **6**-H₂ and **7**-
4 H₂, respectively. For each system, the Soret-like maximum was also red-shifted from ca. 500
5
6 H₂, respectively. For each system, the Soret-like maximum was also red-shifted from ca. 500
7
8 to 600 nm. The calculation results for protonated planar [**455**]-**6**-H₄]²⁺ and [**455**]-**7**-H₄]²⁺
9
10 with B3LYP/6-31g** show the forbidden transitions in the NIR region around 1600 nm
11
12 (Table S1, Table S2). However, the experimental data show the conspicuous absorption
13
14 bands at 1600~1800 nm. Such inconsistency can be attributed to the hydrogen bond
15
16 interactions between pyrrolic protons and TFA counter anions. Because 20 equivalents of
17
18 TFA are added for changing to [**455**]-**6**-H₄]²⁺ and [**455**]-**7**-H₄]²⁺, the hydrogen bond
19
20 interaction may trigger distortion of planar structures and molecular complexes of [**455**]-**6**-
21
22 H₄]²⁺ and [**455**]-**7**-H₄]²⁺ with TFA counter anions which can lead to the intensified lowest
23
24 absorption bands in the NIR region. In the calculation based on the core macrocycle of
25
26 [**455**]-**6**-H₄]²⁺ and [**455**]-**7**-H₄]²⁺, the forbidden transitions in the NIR region exhibited
27
28 increased oscillator strengths when the TFA counter anions are calculated together (Figure
29
30 S55). Thus, it is expected that the hydrogen bonding interactions and formation of molecular
31
32 complexes lead to the enhanced absorption bands in 1600-1800 nm. An additional reaction
33
34 with TFAH could be induced by using a very large excess of acid (300 to 500 equiv). The
35
36 resulting absorption spectra were characterized by a major Q-like absorption in the 900-1200
37
38 nm range. In addition, fluorescence emission was observed in the NIR region at this stage of
39
40 titration (Figure S26). The addition of triethylamine restored quantitatively the free base
41
42 forms **6**-H₂ and **7**-H₂ (Figure S27), indicating the reversibility of the entire acid-induced
43
44 reaction sequence. Spectrophotometric TFAH titrations of **6**-H₂ and **7**-H₂ in dichloromethane
45
46 provided very similar results.
47
48
49
50
51
52
53
54
55
56
57
58
59
60

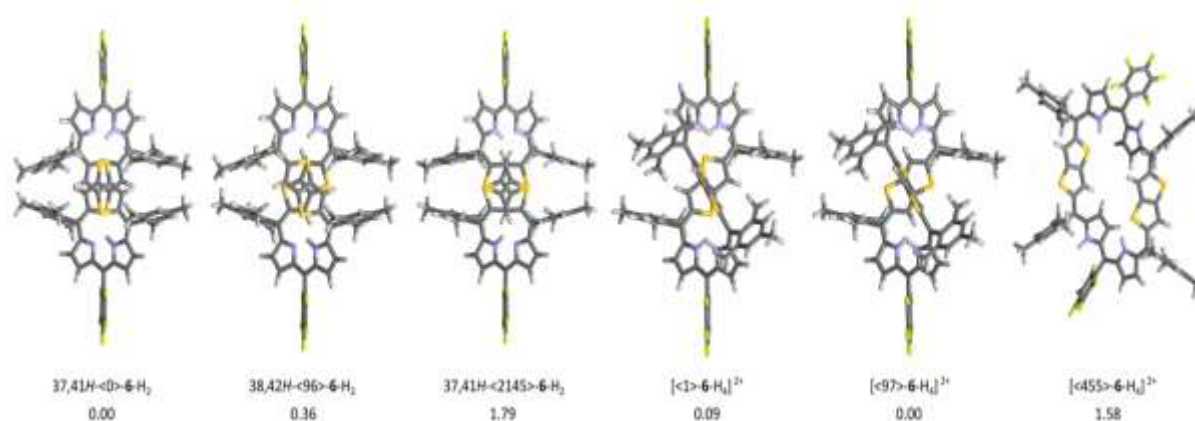


Figure 2 DFT-optimized geometries for selected conformers and tautomers of **6-H₂** and **[6-H₄]²⁺**. Gibbs free energies (PCM(DCM)/KMLYP/6-31G(d,p), kcal/mol, 298 K) are given relative to 37,41H-<0>-**6-H₂** (for free bases), and relative to [**97**]-**6-H₄**²⁺ (for dications).

To gain deeper insight into the change of aromaticity by protonation, we investigated their excited state dynamics by fs-transient absorption (TA) measurements. In line with the changes in the absorption and ¹H NMR spectra of **6-H₂** and **7-H₂** by protonation, their TA spectra also showed drastic spectral changes (Figures 5 and S28). For free base **6-H₂** and **7-H₂**, the TA spectra showed the ground state bleaching (GSB) bands at 520 and 512 nm and the broad excited state absorption (ESA) bands over 550 and 535 nm for **6-H₂** and **7-H₂**, respectively. These TA spectra decayed with two time constants of 0.5 and 15 ps for **6-H₂** and 0.4 and 15 ps for **7-H₂**. The rapid and relatively slow decays in the order of fs and tens of ps suggest the presence of optically dark state typically, which are observed in the TA spectra of antiaromatic porphyrinoids.¹⁰ In accordance with the absorption spectra of **6-H₂** and **7-H₂** with 20 equiv. of TFA, their TA spectra also showed red-shifted GSB and ESA bands. The decay of TA spectra were fitted with the two time constants of 0.2 and 13 ps for **6-H₄²⁺** and 0.1 and 14 ps for **7-H₄²⁺**. Compared to the free base forms, the acceleration of fast time constants are attributable to the more effective π -conjugation with enhanced antiaromaticity on the planar geometries. On the other hand, **6-H₂** and **7-H₂** with 500 equiv. of TFA displayed

1
2
3 the typical features of aromatic porphyrinoids in the TA spectra containing strong GSB band
4 with weak ESA bands.¹⁰ Moreover, the excited state lifetimes were significantly increased.
5
6 Along with their absorption spectra, these observations suggest the Möbius aromatic
7 character of protonated **6**-H₄²⁺ and **7**-H₄²⁺ under excess acid condition. Interestingly, in the
8 comparative analysis between the TA spectra of protonated **6**-H₄²⁺ and **7**-H₄²⁺ under excess
9 acid condition, the clearer TA spectra and longer excited state lifetime were observed for
10 protonated **6**-H₄²⁺. These differences can also be explained on the basis that the mesityl
11 substituents of **6**-H₂ induce more rigidity compared to tolyl substituents of **7**-H₂.
12
13
14
15
16
17
18
19
20
21
22
23

24 To elucidate the conformational changes attendant upon TFAH addition, ¹H NMR
25 spectra were recorded for **6**-H₂ under diverse sets of conditions involving changes of solvent
26 (DCM-*d*₂, 1,2-DCE-*d*₄, acetone-*d*₆), acid concentration (up to ca. 1000 equiv), and
27 temperature. Upon addition of excess trifluoroacetic acid (19 equiv, as 1% solution in DCM-
28 *d*₂, room temperature), dramatic changes in the spectral pattern were observed, consistent
29 with the formation of a dicationic species, **6**-H₄²⁺ (Figures S35-S38).
30
31
32
33
34
35
36
37

38 The occurrence of ring inversion was inferred from the observation of two sets of
39 correlations in 2D COSY spectra (Figure S37), one between a pair of doublets at 16.3–16.9
40 ppm and another between a pair of doublets at 3.7–3.8 ppm, both corresponding to β-CH
41 protons of pyrrole rings. The distinction between the inverted pyrrole and non-inverted
42 pyrrole ring β-CH protons was further based on 2D NOESY spectra (Figure S38). The ¹H
43 NMR spectrum of **6**-H₄²⁺ at 278 K (Figure 6) showed an NH signal at 22.65 ppm, identified
44 by D₂O exchange experiments (Figure S39), which is assumed to correspond to the non-
45 inverted pyrroles. The NH signal of the inverted pyrrole ring is likely broadened by hydrogen
46 bonding and could not be located in the spectrum. The spatial proximity between *o*-methyl
47 protons of one set of Mes groups (2.04 ppm) with adjacent β-CH protons of the noninverted
48 protons of one set of Mes groups (2.04 ppm) with adjacent β-CH protons of the noninverted
49
50
51
52
53
54
55
56
57
58
59
60

1
2
3 pyrrole ring (3.78 ppm) and outer β -CH proton of the thiophene ring (6.94 ppm) produced the
4
5 expected dipolar contacts in the NOESY spectrum, providing unequivocal assignment of the
6
7 three signals. Consequently, the signals at 16.37 and 16.90 ppm were assigned to inner β -CH
8
9 protons of the inverted pyrrole ring. The peak at 15.31 ppm, which showed no correlation
10
11 with any other peak in either COSY or NOESY spectra, was proposed to correspond to the
12
13 inner β -CH proton of thiophene. The two distinct singlets at 6.29 ppm and 6.39 ppm have
14
15 been assigned to the *m*-CH protons of two different *meso*-mesityl rings based on correlations
16
17 that each signal shows to *o*-methyl and *p*-methyl signals in the 2D COSY spectra (Figure
18
19 S37). The observation of inner NH signals at 22.65 ppm is a diagnostic feature of a paratropic
20
21 ring current, which is further manifested in the respectively upfield and downfield shifts of
22
23 other inner and outer protons attached to the macrocycle. These spectral features could be
24
25 rationalized in terms of double pyrrole ring inversion, leading to a quasi-planar conformer
26
27 $[(455)\text{-}6\text{-H}_4]^{2+}$ (Chart 1, Figure 2). An exactly similar NMR spectral pattern has been
28
29 observed upon addition of excess trifluoroacetic acid (19 equiv, as 1% solution in CDCl_3 ,
30
31 room temperature), for 7-H_2 consistent with the formation of a dicationic species, 7-H_4^{2+}
32
33 (Figures S40-S42). Thus, a quasi-planar conformer $[(455)\text{-}7\text{-H}_4]^{2+}$ with two pyrrole ring
34
35 inversion can also be envisaged for 7-H_4^{2+} .
36
37
38
39
40
41
42
43
44
45
46
47
48
49
50
51
52
53
54
55
56
57
58
59
60

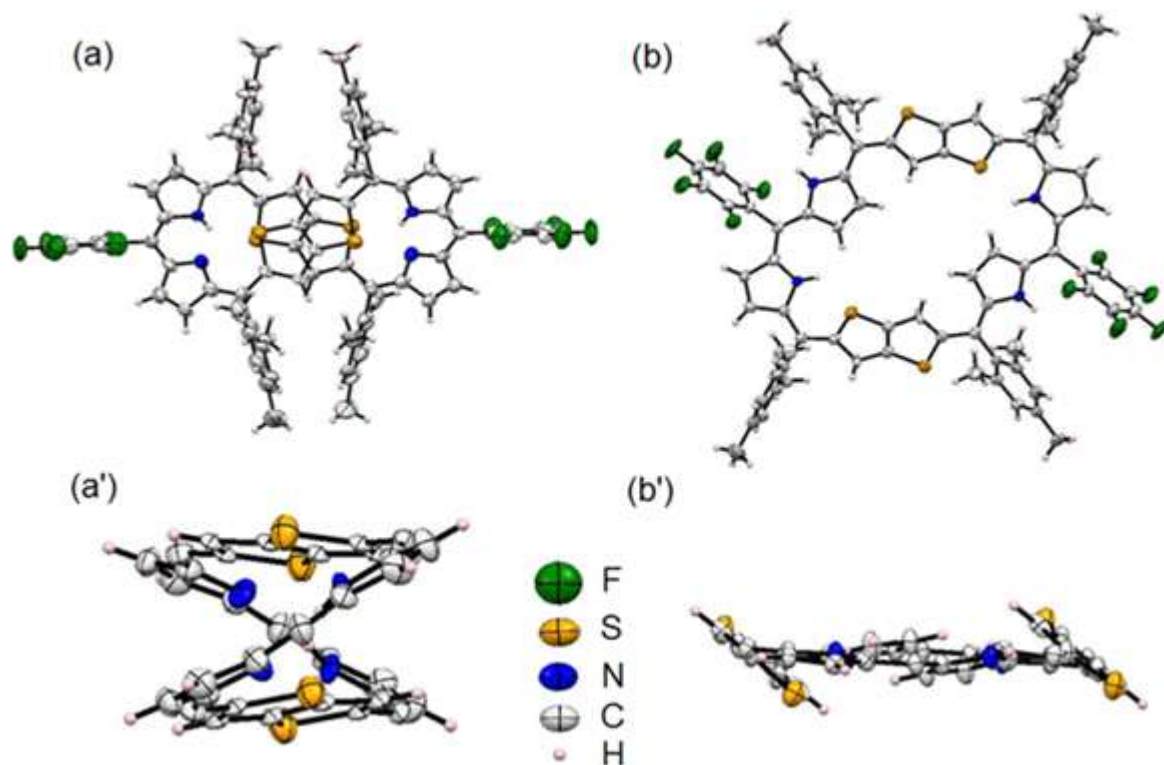


Figure 3. X-ray crystal structure of **6-H₂** in (a) free base, (b) protonated form (a, b: plane view, a', b': side view). The thermal ellipsoids were scaled to the 50% probability level.

Further support for the feasibility of the $\langle 455 \rangle$ conformer was obtained from an X-ray crystallographic analysis. Single crystals of a trifluoroacetate salt [**6-H₄**][CF₃CO₂]₂·[CF₃COOH]₄ were obtained by diffusion of hexane into the CF₃COOH/dichloromethane solution of **6-H₂**. The solid-state geometry of **6-H₄²⁺** was quasi-planar (Figure 3b). There is one centrosymmetric dication in the unit cell, and it is hydrogen-bonded to two dihydrogen tris(trifluoroacetate) assemblies via the NH hydrogens of inverted pyrroles (Figure S56). The inverted pyrrole rings deviated more strongly from the mean plane containing the six *meso* carbons compared to the noninverted pyrrole rings (13.32° vs. 8.56°). The largest tilt was however exhibited by the TT units (38.28°).

Interestingly, when a smaller amount of acid (ca. 1 equiv) is added to the DCM-*d*₂ solution of **6-H₂**, the ¹H NMR spectrum becomes broadened but the positions of peaks remain

virtually unaltered. Likewise, the initial changes of optical absorption spectra are insignificant, indicating that the initial figure-eight conformers **6-H₂** are relatively weak bases. The formation of the $\langle 455 \rangle$ dication requires a double pyrrole ring inversion and is apparently not instantaneous. The rate of ring inversion is accelerated by temperature and by the increasing acid concentration. When a solution of **6-H₂** in DCM-*d*₂ was treated with ca. 35 equiv of TFAH and immediately cooled down to 210 K, a spectrum with effective *D*₂ symmetry was observed (Figure S43), which was clearly distinct from the spectrum of the $\langle 455 \rangle$ dication. Conversion of the *D*₂ intermediate into the $\langle 455 \rangle$ species was however observed when the sample was left to stand at room temperature.

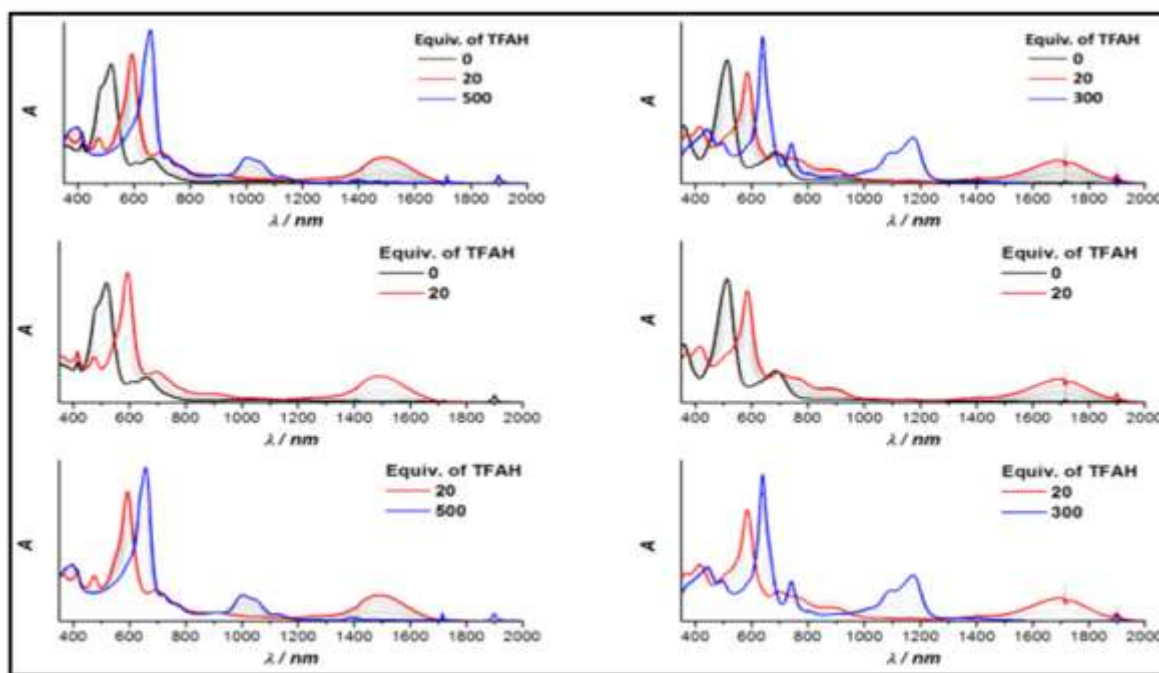


Figure 4. UV-Vis-NIR absorption spectra of (a) **6-H₂** and (b) **7-H₂** upon TFAH titration in 1, 2-dichloroethane.

The transient low-temperature spectrum showed moderate diatropic characteristics, which could be inferred from ¹H shift values, and was thus assumed to correspond to Möbius-type *TI* conformations ($\langle 1 \rangle$ and $\langle 97 \rangle$) in the limit of fast rotation of TT units. Specifically, the

1
2
3 β -CH signals were shifted to 7.30 and 7.19 ppm, whereas a broadened peak, assigned as the
4
5 TT signal, was found at 5.23 ppm. The latter shift, which is dynamically averaged over four
6
7 non-equivalent sites that are present in stationary *TI* structures, is consistent with the upfield
8
9 relocation previously observed in the symmetry-averaged spectra of A, D-di-*p*-
10
11 benziporphyrin.^{4a, b} The Me-*o*-Mes signals in the $\langle 1/97 \rangle$ species resonate at 2.89 and 0.40 ppm.
12
13 While the available 2D NMR data (Figure S44) were insufficient to assign these two peaks,
14
15 they are expected to correspond respectively to exo and endo positions, in line with the
16
17 previously established shielding effects in A, D-di-*p*-benziporphyrin.^{4a, b}
18
19
20
21

22
23 It should be noted that the protonation status of the transient species discussed above
24
25 could not be determined at 210 K, but the formation of the dication is considered probable in
26
27 the presence of a large acid excess. Below 210 K, the spectrum underwent decoalescence,
28
29 consistent with the expected lower symmetries of stationary conformers, but significant line
30
31 broadening precluded more detailed analysis of these complex spectral patterns. Stepwise
32
33 low-temperature titration of **6**-H₂ with TFA produced intermediate spectral patterns of
34
35 considerable complexity, and apparently lower symmetry. DFT-derived ΔG^0_{298} energies
36
37 calculated for $[\langle 1 \rangle\text{-6-H}_4]^{2+}$ and $[\langle 97 \rangle\text{-6-H}_4]^{2+}$ were very similar (0.09 and 0.00 kcal/mol),
38
39 indicating that the two conformers may coexist in solution at experimentally available
40
41 temperatures. The energy of the quasi-planar $\langle 455 \rangle$ system was slightly higher (1.58
42
43 kcal/mol). It should be noted, however, that in these calculations, hydrogen-bonded
44
45 interactions with carboxylate anions and acid molecules were not included. Such interactions
46
47 are expected to be important, especially at high acid concentrations, and have been shown
48
49 previously to affect the conformational dynamics of expanded porphyrins.⁴ Overall, the
50
51 above experimental and theoretical data indicate that the *T2*-type free base of **6**-H₂ does not
52
53 undergo ring inversion when protonated at low temperatures, and the limiting species
54
55
56
57
58
59
60

generated under excess acid conditions is most likely a mixture of Möbius aromatic [$\langle 1 \rangle$]- $\mathbf{6-H}_4^{2+}$ and [$\langle 97 \rangle$]- $\mathbf{6-H}_4^{2+}$ dications.

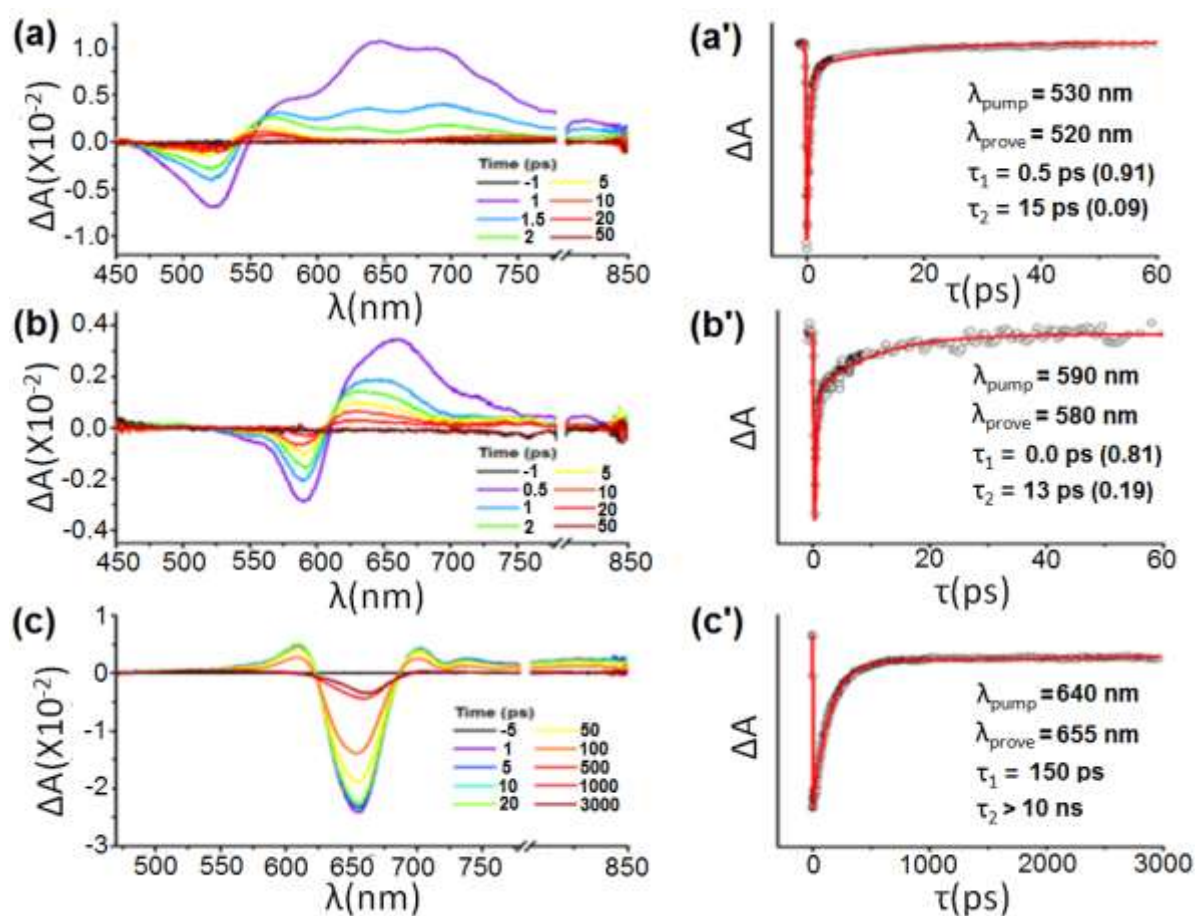


Figure 5. fs-Transient absorption spectra and decay profiles (inset) of $\mathbf{6-H}_2$ with (a) 0, (b) 20 and (c) 500 equiv. of TFAH in 1,2-dichloroethane.

^1H NMR spectra of $[\mathbf{6-H}_4]^{2+}$ obtained in the presence of a very large excess of TFAH (more than 300 equiv) were found to reveal an effective D_2 symmetry and chemical shifts consistent with a diatropic ring current. Such a spectrum was observed in 1, 2-DCE- d_4 at 273 K (Figure S45), when the sample of $\mathbf{6-H}_2$ was treated with ca. 120 equiv of TFAH. When the amount of acid was gradually increased to ca. 1000 equiv the spectrum became sharper. The ^1H shifts underwent only minor changes of chemical shifts, likely resulting from interactions with excess TFAH (final values: $\beta\text{-H}$ 7.21 and 7.15 ppm, TT 5.99 ppm, NH 5.84 ppm). A

1
2
3 sharp, high symmetry spectrum, with similar shifts (β -H 7.53 and 7.09 ppm, TT 6.37 ppm,
4
5 NH not observed, *o*-Mes 2.85, 0.60, *m*-Mes 7.20, 6.62, *p*-Mes 2.23 ppm, Figure S47) was
6
7 also observed in acetone-*d*₆ in the presence of TFAH (ca. 20% v/v). The associated electronic
8
9 absorption spectrum was however different in comparison with the DCE experiment: while
10
11 the position of the Soret band was preserved, the Q bands were observed in the 800–1000 nm
12
13 range in the acetone solution (Figure S24). In acetone-*d*₆, exchange cross-peaks between endo
14
15 and exo positions of the Mes group were observed for [6-H₄]²⁺ in the ROESY spectrum
16
17 (Figure S49), indicating a slow untwisting of the figure-eight structure. On lowering the
18
19 temperature, gradual line broadening was observed, but the symmetry of the spectrum
20
21 remained unchanged down to 170 K.
22
23
24
25
26

27 The ¹H NMR spectrum of [6-H₄]²⁺ observed in the presence of a large acid excess is
28
29 very similar to that observed for the transient ⟨1/97⟩ conformer generated at low temperature,
30
31 and it is tempting to suggest that the conformation of the high excess acid species might in
32
33 fact be the same. While such an interpretation is most likely, it should be noticed that the ¹H
34
35 NMR spectrum is in all cases being observed in the limit of fast exchange, and exact
36
37 structures of these conformers are not accessible. In particular, the conformational changes
38
39 induced at different acid concentrations may involve not only rotations of TT units (which
40
41 generate the ⟨0, 1, 96, 97, 2145⟩ conformers, and are sufficient to induce topology switching)
42
43 but also additional twists of the macrocycle near pyrrole rings. As long as such a twist does
44
45 not lead to a complete inversion of the figure-eight structure, a *D*₂ symmetric spectrum is
46
47 expected in the fast exchange limit. Nevertheless, the symmetry-averaged ¹H shifts observed
48
49 at high acid concentrations are consistent with a moderately diatropic structure, as indicated
50
51 by the downfield positions of β -H signals ($\delta > 7$ ppm), and the unusually upfield position of
52
53 the TT signal. The latter change is similar to that observed for the *p*-phenylene signal in the
54
55 ¹H NMR spectrum of A,D-di-*p*-benzihexaphyrin^{4a}, and may thus indicate a Möbius-type *TI*
56
57
58
59
60

conformer. In line with the latter conjecture, the ^1H NMR shifts of $[\mathbf{6}\text{-H}_4]^{2+}$ measured in acetone- d_6 are in a semi-quantitative yet still remarkably good agreement with the D_2 -averaged GIAO shieldings calculated for the lowest-energy dication $\langle 97 \rangle\text{-}[\mathbf{6}\text{-H}_4]^{2+}$ (Figure S50). In particular, the calculation correctly reproduces the downfield relocations of $\beta\text{-H}$ signals and the upfield position of TT (7.02 ppm), relative to the T2 free base.

The conformational change observed at different acid concentrations is most likely promoted by association of TFA anions and TFAH molecules to the $[\mathbf{6}\text{-H}_4]^{2+}$, in analogy to the behavior observed for A,D-di-*p*-benzporphyrin in the presence of dichloroacetic acid.^{4b} However, since the present system is observed only in the fast exchange limit, the exchange between bulk and associated acid molecules and anions results in the complete loss of any structural information related to the acid binding and symmetry averaging of the ^1H NMR spectral pattern of $[\mathbf{6}\text{-H}_4]^{2+}$.

In different solvents and at different acid concentrations, the stationary geometries are likely to differ because of hydrogen-bonded interactions with TFAH molecules. Acid association in solution was previously demonstrated for A,D-di-*p*-benzihexaphyrin^{4b} as well as for other porphyrinoid systems.⁴ Association with TFAH is expected to be significantly stronger in DCE (and DCM) than in acetone, because of the higher polarity of the latter solvent, and may explain why the absorption spectrum of $[\mathbf{6}\text{-H}_4]^{2+}$ in acetone is different.

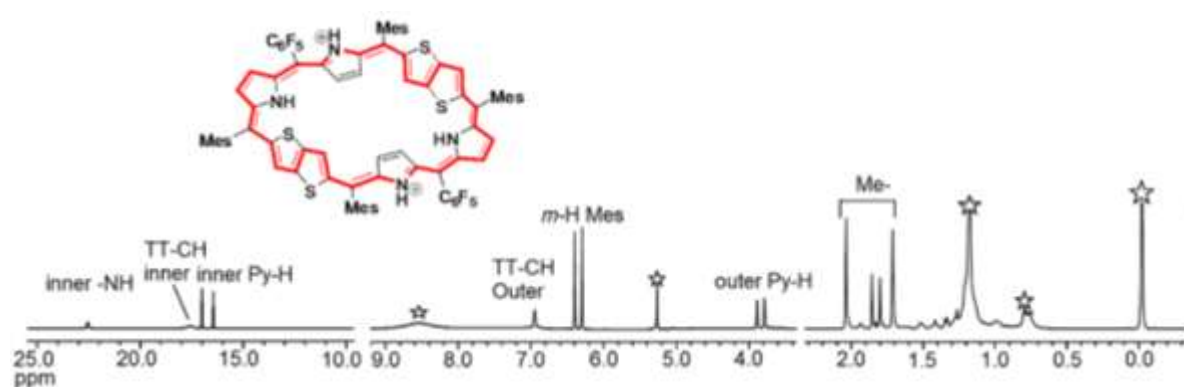
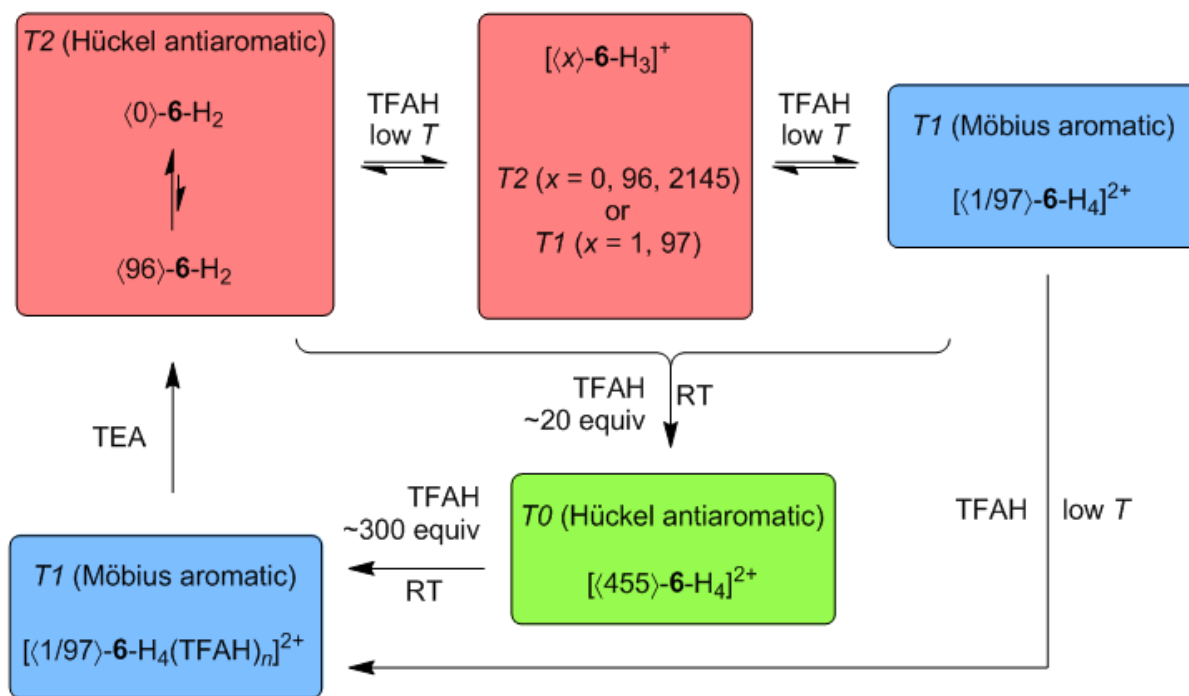


Figure 6. ^1H NMR spectrum of protonated $\mathbf{6}\text{-H}_4^{2+}$ in CD_2Cl_2 at 278 K.



Scheme 2. Acid-base and conformational behavior of **6-H₂** in 1, 2- DCE.

The conformational behavior of **6-H₂** in DCE at various acid concentrations is summarized in Scheme 2. When the protonation is performed at low temperatures (below ca. 273 K with rapid acid addition), the figure-eight twist of the macrocycle is preserved, and the system goes from the *T2* free base structure (the $\langle 0/96 \rangle$ equilibrium mixture) via an unspecified mixture of *T2* and *T1* conformations at the monocation level to the predominantly *T1*-type dication. The spectral symmetry of this species and its diatropic character are retained over a wide range of acid concentrations, implying that the conformation is preserved. However, extensive association with acid molecules is indirectly observed above 100 equiv of TFAH. When **6-H₂** is titrated at room temperature, the dication undergoes double pyrrole inversion in the initial titration phase, to yield the quasi-planar $[\langle 455 \rangle\text{-6-H}_4]^{2+}$ species. The latter conformer is stable up to ca. 20 equiv of TFAH, but it reverts to the figure-eight Möbius structure $[\langle 1/97 \rangle\text{-6-H}_4]^{2+}$, when more acid is added. A qualitatively similar behavior was observed for **7-H₂** upon titration with TFAH in dichloromethane-*d*₂ (Figure

1
2
3 S51), but the system was less amenable to 2D spectral analysis (Figure S53). A spectrum
4
5 clearly corresponding to the *T2* conformer [$\langle 455 \rangle$ -7-H₄]²⁺ was observed at intermediate acid
6
7 concentrations. In the presence of a large excess of TFAH, the appearance of the spectrum
8
9 indicated the presence of multiple forms. The major species observed at 263–243 K (Figure
10
11 S52) could however be identified as a *D*₂-symmetric diatropic structure β -pyrroles: 8.06, 7.96
12
13 ppm, TT 5.87 ppm, Figure S54). In particular, this species features a single set of signals
14
15 corresponding to a slowly rotating Tol substituent (*ortho* 8.13, 6.21 ppm, *meta* 7.28, 7.11
16
17 ppm, *p*-Me 2.33 ppm). This result is again consistent with the prevalence of a Möbius species
18
19 at high acid concentrations proposed above for 7-H₂ on the basis of TA spectroscopy.
20
21
22
23
24
25
26
27
28
29

30 CONCLUSION

31
32
33
34 In conclusion, the present manuscript provides many insights into the conformational
35
36 behavior of a highly twisted fused [32] heteroannulene associated with various topologies.
37
38 Excellent agreement between the theoretically determined properties and the experimental
39
40 spectroscopic measurements are key to the evidence of weak twisted-Hückel antiaromatic,
41
42 strongly Hückel antiaromatic and Möbius aromatic states respectively upon stepwise
43
44 protonation. Our results are in accordance with the fact that protonation disrupts
45
46 intramolecular H-bonding thereby leading to topological dichotomy in order for the
47
48 macrocycle to gain aromatic stabilization energy. Further development of dynamic
49
50 heteroannulenes is currently under progress in our laboratory.
51
52
53
54
55
56
57
58
59
60

EXPERIMENTAL SECTION

Materials and Methods:

Electronic absorption spectra were measured with a UV-vis-NIR spectrophotometer, and variable temperature UV-vis-NIR were carried out in cryostat. ^1H , and ^{13}C NMR spectra were recorded on a spectrometer (operating as 600.17 MHz for ^1H and 150.91 MHz for ^{13}C) using the residual solvents as the internal references for ^1H [(CHCl_3 ($\delta = 7.26$ ppm), CH_2Cl_2 ($\delta = 5.32$ ppm), Acetone ($\delta = 2.04$ ppm) and DCE ($\delta = 3.72$ ppm)].

High-resolution electrospray ionization time-of-flight mass spectroscopy (HR-ESI-TOF MS) was conducted by using the positive mode for an acetonitrile solution of samples. All solvents and chemicals were of reagent grade quality, obtained commercially and used without further purification except as noted. For spectral measurements, anhydrous dichloromethane was obtained by refluxing and distillation over CaH_2 . Dry THF was obtained by refluxing and distillation over pressed Sodium metal. Thin layer chromatography (TLC) was carried out on alumina sheets coated with silica gel 60 F₂₅₄ and gravity column chromatography were performed using Silica Gel 230-400 mesh.

X-Ray structure determination

Crystallographic data were collected at 100 K by using graphite-monochromated Mo-K α ($\lambda = 0.71073\text{\AA}$). The structures were solved by SHELX-2014 using SHELXTL suite of programme. The final refinement of the structure was carried out using least-squares method on F^2 using SHELXL-2014. The final refinement of the solved structure converged at the R value of 0.0856 ($I > 2\sigma(I)$) for free base form of **6**-H₂ and R value of 0.0737 ($I > 2\sigma(I)$) for protonated form of **6**-H₄²⁺ and R value of 0.0677 ($I > 2\sigma(I)$) for free base **7**-H₂. All non-hydrogen atoms were refined anisotropically. All the hydrogen atoms were located from

1
2
3 difference Fourier maps. For protonated **6**-H₄²⁺, ALERT 2A, 2B arises from potentially
4
5 disordered solvent molecules. We tried to fix by using PART command, however atomic
6
7 displacement values didn't reduce.
8
9

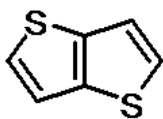
11 **Femtosecond transient absorption measurements**

12
13
14 The femtosecond transient absorption (fs-TA) spectra were measured with a spectrometer
15
16 consisting of two independently tunable homemade optical parametric amplifiers (OPAs)
17
18 pumped by a regeneratively amplified Ti: sapphire laser system operating at a repetition rate
19
20 of 1 kHz and an optical detection system.
21
22
23
24
25
26
27

28 **Theoretical Calculation**

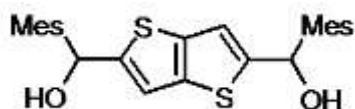
29
30
31 Density functional theory (DFT) calculations were performed using Gaussian 09.¹¹ DFT
32
33 geometry optimizations were carried out in unconstrained C₁ symmetry, using molecular
34
35 mechanics or semiempirical models as starting geometries. DFT geometries were refined to
36
37 meet standard convergence criteria, and the existence of a local minimum was verified by a
38
39 normal mode frequency calculation. DFT calculations were performed using the KMLYP
40
41 functional¹² and the 6-31G (d, p) basis set. PCM solvation (dichloromethane
42
43 parameterization) was included in all calculations. NMR chemical shifts were calculated
44
45 using the GIAO/KMLYP/6-31G (d, p) level of theory. The absolute shielding of TMS
46
47 calculated at the KMLYP level of theory was 31.946 ppm. Electronic absorption spectra were
48
49 calculated using time-dependent DFT in the Tamm–Dancoff approximation, using the
50
51 B3LYP functional and dichloromethane solvation. Up to 50 transitions were calculated,
52
53 providing full coverage of the NIR and visible regions.
54
55
56
57
58
59
60

SYNTHESIS



Thieno[3,2-b]thiophene (1): This was synthesized as reported in literature.

Yield: 60 %. Colourless crystalline solid. M.p. 53-58 °C. ^1H NMR (300 MHz, CDCl_3): δ [ppm]: 7.26-7.28 (d, 2H, $J = 4.8$ Hz); 7.38-7.40 (d, 2H, $J = 5$ Hz). ^{13}C NMR (75 MHz, CDCl_3 , 300K, δ [ppm]): 119.6, 127.6, 139.7. **HR-ESI-TOF MS (m/z):** Found 162.9631 $[\text{M}+\text{Na}]^+$ (Calcd. 162.9647 for $\text{C}_6\text{H}_4\text{S}_2\text{Na}^+$). Anal. Calcd for $\text{C}_6\text{H}_4\text{S}_2$: C, 51.39; H, 2.88. Found: C, 51.41; H, 2.90.

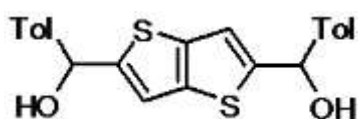


(2, 5-Bis (mesitylhydroxymethyl)-thieno [3, 2-b]thiophene

(2): To a 250 mL round-bottomed flask equipped with a magnetic bar, thieno [3, 2-b] thiophene **5** (1 g, 7.13 mmol) was placed followed by dry THF (40 mL). The reaction mixture was stirred under inert atmosphere. N, N, N', N'-Tetramethyl ethylenediamine (3.2 mL, 0.021 mol) was added followed by stirring for half an hour at room temperature. Afterward n-BuLi in hexane (1.6 M) (13.04 mL, 0.021 mol) was added through rubber septa drop wise, yellow turbidity started forming. The reaction mixture was stirred at room temperature for 2 hours and then heated to 66°C for 1 hour. The reaction mixture was brought room temperature after which it was brought to ice cold temperature. At ice cold temperature, Mesitaldehyde (2.62 mL, 0.017 mol) in dry THF (40 mL) was then added drop wise to the reaction mixture, the reaction mixture was stirred for 2 hours. The reaction mixture was quenched by saturated NH_4Cl (aq) solution, product was extracted by diethyl ether, dried over Na_2SO_4 . The crude product was precipitated out by hexane and purified by

silica gel column chromatography using ethyl acetate-hexane (1:4) solution. The solvent was evaporated and light yellow solid was obtained.

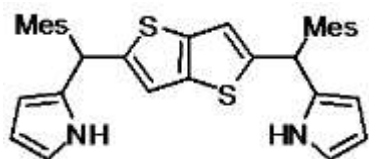
Yield 2.09 g (67%). M.p. 156 °C. ¹H NMR (500 MHz, CDCl₃, 300K, δ [ppm]): 2.28 (s, 6H); 2.33 (s, 12H); 6.46 (s, 2H); 6.71 (s, 2H); 6.87 (s, 4H); ¹³CNMR (125 MHz, CDCl₃, 300K, δ [ppm]): 20.6, 29.8, 69.8, 116.4, 130.2, 135.3, 137.0, 137.9, 138.3, 148.8. HR-ESI-TOF MS (m/z): Found 459.1430 [M+Na]⁺ (Calcd. 459.1423 for [C₂₆H₂₈O₂S₂Na]⁺). Anal. Calcd for C₂₆H₂₈O₂S₂: C, 71.52; H, 6.46. Found: C, 71.50; H, 6.44.



(2,5-Bis(tolyhydroxymethyl)-thieno[3,2-b]thiophene (3):

To a 250 mL round-bottomed flask equipped with a magnetic bar, thieno[3,2-b]thiophene **5** (1 g, 7.13mmol) was placed followed by dry THF (40 mL). The reaction mixture was stirred under inert atmosphere. N, N, N', N'-Tetramethyl ethylenediamine (3.2 mL, 0.021 mol) was added followed by stirring for half an hour at room temperature. Afterward n-BuLi in hexane (1.6 M) (13.04 mL, 0.021 mol) was added through rubber septa drop wise, yellow turbidity started forming. The reaction mixture was stirred at room temperature for 2 hours and then heated to 66 °C for 1hour. The reaction mixture was brought room temperature after which it was brought to ice cold temperature. At ice cold temperature, *p*-tolylaldehyde (2 mL, 0.017 mol) in dry THF (40 mL) was then added drop wise to the reaction mixture, the reaction mixture was stirred for 2 hours. The reaction mixture was quenched by saturated NH₄Cl (aq) solution, product was extracted by diethyl ether, dried over Na₂SO₄. The crude product was precipitate out by hexane and purified by silica gel column chromatography using ethyl acetate-hexane (1:4) solution. The solvent was evaporated and light yellow solid was obtained.

Yield 2.09 g (77.5%). M.p. 135 °C. $^1\text{H NMR}$ (500 MHz, CDCl_3 , 300K, δ [ppm]): 2.35 (s, 6H); 6.02 (s, 2H); 6.97 (s, 2H); 7.17-7.18 (d, 4H, $^3J = 8$ Hz); 7.33-7.34 (d, 4H, $^3J = 8$ Hz). $^{13}\text{CNMR}$ (125 MHz, CDCl_3 , 300K, δ [ppm]): 29.8, 73.1, 117.5, 126.4, 129.3, 138.1, 138.3, 139.6, 150.1. **HR-ESI-TOF MS (m/z):** Found 403.0793 $[\text{M}+\text{Na}]^+$ (Calcd. 403.0797 for $[\text{C}_{22}\text{H}_{20}\text{O}_2\text{S}_2\text{Na}]^+$). Anal. Calcd for $\text{C}_{22}\text{H}_{20}\text{O}_2\text{S}_2$: C, 69.44; H, 5.30. Found: C, 69.46; H, 5.32.



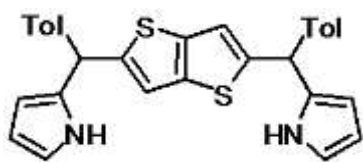
2-(mesityl (1H-pyrrole-2-yl) methyl) thieno[3, 2-

b]thiophene-5-yl) methyl)-1H-pyrrole (4): Compound **2** (1g, 2.29 mmol) was dissolved in pyrrole (15 mL, 0.19 mol). The solution was stirred for 45 minutes under nitrogen atmosphere at room temperature. Trifluoroacetic acid (0.05 mL, 0.22 mmol) was added and stirred for 1hour. The reaction mixture was quenched by dichloromethane; product was neutralized by NaOH (aq) solution, extracted by dichloromethane, dried over Na_2SO_4 and dried in rotary evaporator to give yellow oil. The crude product was purified by silica gel chromatography using 10% ethylacetate-hexane mixture. Compound **4** was obtained as light yellow foam.

Yield 0.702 g (57%). $^1\text{H NMR}$ (500 MHz, CDCl_3 , 300K, δ [ppm]): 2.03 (s, 6H, -Me); 2.29-2.35 (s, 12H, -Me); 4.24 (s, 2H, -CH); 6.03 (br, 1H, β -H of pyrrole); 6.13 (s, 1H, β -H of thienothiophene); 6.23 (d, 1H, $J = 4.5$ Hz, β -H of pyrrole); 6.30 (d, 1H, $J = 4.5$ Hz, β -H of pyrrole); 6.54 (br, 1H, β -H of pyrrole); 6.69 (s, 1H, β -H of thienothiophene); 6.70-6.71 (m, 1H, β -H of pyrrole), 6.72-6.73 (m, 1H, β -H of pyrrole); 6.86 (s, 2H, Mesityl-CH); 6.92 (s, 2H, Mesityl-CH); 7.99 (br, 1H, -NH); 8.50 (br, 1H, -NH). $^{13}\text{CNMR}$ (125 MHz, CDCl_3 , 300K, δ [ppm]): 20.1, 20.7, 20.9, 21.1, 30.8, 41.2, 107.4, 108.5, 109.2, 109.4, 117.0, 117.4, 118.9, 124.7, 126.3, 129.2, 130.6, 133.3, 134.0, 135.9, 136.4, 136.5, 136.8, 137.0, 137.1,

1
2
3
4
5
6
7
8
9
10
11
12
13
14
15
16
17
18
19
20
21
22
23
24
25
26
27
28
29
30
31
32
33
34
35
36
37
38
39
40
41
42
43
44
45
46
47
48
49
50
51
52
53
54
55
56
57
58
59
60

137.2, 137.5, 145.5. **HR-ESI-TOF MS (m/z):** Found 534.2145 [M^+] (Calcd. 534.2163 for $[C_{34}H_{34}N_2S_2]^+$). Anal. Calcd for $C_{34}H_{34}N_2S_2$: C, 76.36; H, 6.41, N, 5.24. Found: C, 76.39; H, 6.45; N, 5.20.



2-(tolyl (1H-pyrrole-2-yl) methyl) thieno[3, 2-b]thiophene-5-

yl) methyl-1H-pyrrole (**5**): Following the synthetic procedure described for **4**, **5** was obtained starting from **3**.

Yield 0.895 g (81%). 1H NMR (500 MHz, $CDCl_3$, 300K, δ [ppm]): 2.38 (s, 6H, -Me); 5.63 (s, 2H, -CH); 5.97 (br, 2H, β -H of pyrrole); 6.86 (s, 2H, β -H of thienothiophene); 6.69 (d, 2H, $J = 4.5$ Hz, β -H of pyrrole); 6.70 (d, 2H, $J = 4.5$ Hz, β -H of pyrrole); 7.16 (d, 4H, $J = 10$ Hz, CH-Tolyl); 7.12 (d, 4H, $J = 10$ Hz, CH-Tolyl); 7.91 (br, 2H, -NH). ^{13}C NMR (125 MHz, $CDCl_3$, 300K, δ [ppm]): 21.2, 46.5, 107.8, 108.6, 117.3, 118.4, 128.4, 129.4, 132.9, 137.0, 137.8, 139.5, 148.7. **HR-ESI-TOF MS (m/z):** Found 478.1567 [M^+] (Calcd. 478.1537 for $[C_{30}H_{26}N_2S_2]^+$). Anal. Calcd for $C_{30}H_{26}N_2S_2$: C, 75.28; H, 5.47; N, 5.85. Found: C, 75.29; H, 5.49; N, 5.84.

General synthetic procedure of Compound 6-H₂: Under nitrogen atmosphere and in dark condition a solution of 534mg of compound **4** (1mmol) and pentafluorobenzaldehyde (0.12mL, 1mmol) in 250 mL dry dichloromethane was stirred for 30 minutes. Afterward, catalytic amount of p-TSA (95mg) was added to the reaction mixture and stirred at RT for 90 minutes. Then chloranil (490mg, 1.99 mmol) was added and opened to air and the mixture was refluxed for another 1 hour. The solvent was removed under reduced pressure and compound was filtered by basic alumina followed by repeated silica gel column

1
2
3 chromatography with the mixture of 40% dichloromethane - hexane solution. After
4
5 recrystallization, the title compound was yielded as dark red crystal.
6
7

8
9 Yield.~85mg (~6%). M.p.>350 °C. **MALDI-TOF MS (m/z):** Found 1416.3415 (Calcd.
10
11 1416.3385 for [C₈₂H₅₈F₁₀N₄S₄]⁺). **UV-VIS (CH₂Cl₂, λ [nm], (ε [M⁻¹ cm⁻¹x10³]), 298K):**
12
13 517(43.79); 658 (8.56). Anal. Calcd for C₈₂H₅₈F₁₀N₄S₄: C, 69.47; H, 4.12; N, 3.95. Found: C,
14
15 69.48; H, 4.15; N, 3.93.
16
17

18
19 **¹H NMR (600 MHz, CD₂Cl₂, 193 K, δ [ppm], TMS):** 1.45 (s, *exo-o*-Mes), 2.41 (s, *p*-CH₃);
20
21 3.27 (s, *endo-o*-Mes); 5.81 (brs, pyrrole β-H); 6.62 (brs, pyrrole β-H) ;6,87 (brs, *exo-m*-
22
23 Mes); 7.20 (s, -CH TT); 7.47 (brs, *endo-m*-Mes)); 9.96 (s, TT β-H <96>); 17.75 (brs, s,
24
25 <0>NH); 18.61 (s, <96>NH).
26
27
28

29
30 **¹H NMR (600 MHz, 1% CF₃COOH/CD₂Cl₂, 273 K, δ [ppm], TMS):** 1.70 (s, *o*-CH₃); 1.81
31
32 (s, *p*-CH₃); 1.86 (s, *p*-CH₃); 2.04 (s, *o*-CH₃); 3.78 (d, J = 3.5, 1H, pyrrole β-H) ; 3.88 (d, J
33
34 =4.2, 1H, pyrrole β-H); 6.29 (s, -CH mesityl); 6.39 (s, -CH mesityl); 6.94 (s, TT β-H); 16.37
35
36 (brs, pyrrole β-H); 16.90 (brs, pyrrole β-H); 17.21 (s, TT β-H); 22.52 (s, -NH).
37
38
39

40
41 **General synthetic procedure of Compound 7-H₂:** Under nitrogen atmosphere and in dark
42
43 condition a solution of 478 mg of compound **5** (1mmol) and pentafluorobenzaldehyde (0.12
44
45 mL, 1mmol) in 250 mL dry dichloromethane was stirred for 30 minutes. Afterward, catalytic
46
47 amount of *p*-TSA (95 mg) was added to the reaction mixture and stirred at RT for 90 minutes.
48
49 Then chloranil (490 mg, 1.99 mmol) was added and opened to air and the mixture was
50
51 refluxed for another 1 hour. The solvent was removed under reduced pressure and compound
52
53 was filtered by basic alumina followed by repeated silica gel column chromatography with
54
55 the mixture of 40% dichloromethane - hexane solution. After recrystallization, the title
56
57 compound was yielded as dark red crystal.
58
59
60

1
2
3 Yield. ~110mg (~8%). M.p.> 350 °C. **MALDI -TOF MS (m/z):** Found 1304.2170 (Calc.
4
5 1304.2133 for [C₇₄H₄₂N₄F₁₀S₄]⁺). **UV-VIS (CH₂Cl₂, λ [nm], (ε [M⁻¹ cm⁻¹x10³]), 298K):**
6
7 511(50.65); 683 (8.15). Anal. Calcd for C₇₄H₄₂N₄F₁₀S₄: C, 68.09; H, 3.24; N, 4.29. Found: C,
8
9 68.11; H, 3.25; N, 4.27.
10
11
12

13
14
15 **¹H NMR (600 MHz, CD₂Cl₂, 213 K, δ [ppm], TMS):** 2.46-2.52 (s, *p*-CH₃); 6.04 (d, pyrrole
16
17 β-H); 6.30 (d, pyrrole β-H); 7.28-7.37 (Tol-CHs); 7.81 (s, -CH TT); 9.98 (s, TT β-H <96>);
18
19 17.50 (brs, s, <0>NH); 17.98 (s, <96>NH).
20
21
22

23
24 **¹H NMR (500 MHz, 1% CF₃COOH/CDCl₃, 288 K, δ [ppm], TMS):** 2.24 (s, 6H, *p*-CH₃); 2.28
25
26 (s,6H, *p*-CH₃); 5.22 (d, J = 4.5, 2H, pyrrole β-H); 5.64 (d, 2H, J = 5, pyrrole β-H); 6.08 (s, 2H, TT β-
27
28 H); 6.50 (d, 4H, J = 7.5, Toly-H); 6.74 (d, 4H, J = 8, Toly-CH); 6.89 (d, 4H, J = 8, Toly-CH); 7.00
29
30 (d, 4H, J = 8, Toly-CH); 12.78 (s, 2H, pyrrole β-H); 13.11 (s, 2H, pyrrole β-H); 13.15 (s, 2H, TT β-
31
32 H); 17.38 (brs, 2H, pyrrole -NH).
33
34
35

36 ASSOCIATED CONTENT

37 38 39 ACKNOWLEDGEMENTS

40
41
42
43
44 The work at IACS, Kolkata was supported by DST-SERB (SR/S1/IC-37/2012) and DST-
45
46 SERB Ramanujan Fellowship (SR/S2/RJN-93/2011), India. AM thanks CSIR for senior
47
48 research fellowship. The work at Yonsei University was supported by the Global Research
49
50 Laboratory Program (2013K1A1A2A02050183) funded by the Ministry of Science, ICT &
51
52 Future, Korea. Financial support from the National Science Center of Poland (grant
53
54 2014/13/B/ST5/04394 to M.S.) is gratefully acknowledged. Quantum chemical calculations
55
56 were performed in the Centers for Networking and Supercomputing of Wrocław and
57
58 Poznań. We are indebted to the Single Crystal X-Ray Diffractometer facility in NISER,
59
60

Bhubaneswar, Odisha, India. We sincerely thank Dr. Palani Sasikumar, Presidency University, Kolkata, India for final refinement of crystal data reported in this manuscript.

Supporting Information

The Supporting Information is available free of charge on the ACS Publications website.

Scheme, HR-ESI-TOF mass spectra, MALDI-TOF mass spectra, NMR spectra (^1H NMR, ^{13}C NMR, acid titration, variable temperature, ^1H - ^1H COSY, ^1H - ^1H ROESY, ^1H - ^1H NOESY), details of absorption spectroscopic (solvent dependent, acid titration, variable temperature study), results of DFT calculations, TA spectra, X-ray crystallographic details, and Cartesian Coordinates.

REFERENCES

- (1) Turro, N. J. *Angew. Chem. Int. Ed.* **1986**, *25*, 882.
- (2) (a) Rzepa, H. S. *Chem. Rev.* **2005**, *105*, 3697. (b) Herges, R. *Chem. Rev.* **2006**, *106*, 4820.
(c) Heilbronner, E. *Tetrahedron Lett.* **1964**, *5*, 1923. (d) Ajami, D.; Oeckler, O.; Simon, A.; Herges, R. *Nature* **2003**, *426*, 819. (e) Schaller, G. R.; Topić, F.; Rissanen, K.; Okamoto, Y.; Shen, J.; Herges, R. *Nat. Chem.* **2014**, *6*, 608.
- (3) (a) Sessler, J. L.; Weghorn, S. J. *Expanded, Contracted and Isomeric Porphyrins*, Pergamon, New York, **1997**, *15*, 429. (b) Chandrashekar, T. K.; Venkatraman, S. *Acc. Chem. Res.* **2003**, *36*, 676. (c) Sessler, J. L.; Seidel, D. *Angew. Chem. Int. Ed.* **2003**, *42*, 5134. (d) Saito, S.; Osuka, A. *Angew. Chem. Int. Ed.* **2011**, *50*, 4342. (e) Stępień, M.; Sprutta, N.; Latos-Grażyński, L. *Angew. Chem. Int. Ed.* **2011**, *50*, 4288. (f) Sung, Y. M.; Yoon, M.-C.; Lim, J. M.; Rath, H.; Naoda, K.; Osuka, A.; Kim, D. *Nat. Chem.* **2015**, *7*, 418. (g) Oh, J.; Mori, H.; Sung, Y. M.; Kim, W.; Osuka, A.; Kim, D. *Chem. Sci.* **2016**, *7*, 2239.

- 1
2
3
4
5
6
7
8
9
10
11
12
13
14
15
16
17
18
19
20
21
22
23
24
25
26
27
28
29
30
31
32
33
34
35
36
37
38
39
40
41
42
43
44
45
46
47
48
49
50
51
52
53
54
55
56
57
58
59
60
- (4) (a) Stępień, M.; Sprutta, N.; Chwalisz, P-; Szterenber, L.; Latos-Grażyński, L. *Angew. Chem. Int. Ed.* **2007**, *46*, 7869. (b) Stępień, M.; Szyszko, B.; Latos-Grażyński, L. *J. Am. Chem. Soc.* **2010**, *132*, 3140. (c) Rappaport, S. M.; Rzepa, H. S. *J. Am. Chem. Soc.* **2008**, *130*, 7613. (d) Szyszko, B.; Sprutta, N.; Chwalisz, P-; Stępień, M.; Latos-Grażyński, L. *Chem. Eur. J.* **2014**, *20*, 1985. (e) Yoon, Z. S.; Osuka, A.; Kim, D. *Nat. Chem.* **2009**, *1*, 113 and references therein. (f) Latos-Grazynski, L. et al. *Phys. Chem. Chem. Phys.* **2015**, *17*, 6644. (g) Cha, W. -Y.; Soya, T.; Tanaka, T.; Mori, H.; Hong, Y.; Lee, S.; Park, K.H.; Osuka, A.; Kim, D. *Chem. Commun.* **2016**, *52*, 6076. (h) Mallick, A.; Rath, H. *Chem. Asian. J.* **2016**, *11*(7), 986. (i) Ghosh, A.; Chaudhury, A.; Srinivasan, A.; Suresh, C. H.; Chandrashekar, T. K. *Chem. Eur. J.* **2016**, *22*, 3942.
- (5) (a) Lim, J. M.; Shin, J-Y.; Tanaka, Y.; Saito, S.; Osuka, A.; Kim, D. *J. Am. Chem. Soc.*, **2010**, *132*(9), 3105. (b) Saito, S.; Shin, J-Y.; Lim, J. M.; Kim, K. S.; Kim, D.; Osuka, A. *Angew. Chem. Int. Ed.* **2008**, *47*, 9657. (c) Kido, H.; Shin, J. -Y.; Shinokubo, H. *Angew. Chem. Int. Ed.* **2013**, *52*, 13727. (d) Tanaka, Y.; Saito, S.; Mori, S.; Aratani, N.; Shinokubo, H.; Shibata, N.; Higuchi, Y.; Yoon, Z. S.; Kim, K. S.; Noh, S. B.; Park, J. K.; Kim, D.; Osuka, A. *Angew. Chem. Int. Ed.* **2008**, *47*, 681. (e) Alonso, M.; Pinter, B.; Geerlings, P.; Proft, F. D. *Chem. Eur. J.* **2015**, *21*, 17631. (f) Yoon, M.-C.; Shin, J.-Y., Lim, J. M.; Saito, S.; Yoneda, T.; Osuka, A.; Kim, D. *Chem. Eur. J.* **2011**, *17*, 6707. (g) Alonso, M.; Geerlings, P.; Proft, F. D. *Chem. Eur. J.* **2012**, *18*, 10916.
- (6) (a) Karthik, G.; Lim, J. M.; Srinivasan, A.; Suresh, C. H.; Kim, D.; Chandrashekar, T. K. *Chem. Eur. J.* **2013**, *19*, 17011. (b) Rath, H.; Sankar, J.; Prabhuraja, V.; Chandrashekar, T. K.; Joshi, B. S.; Roy, R. *Chem. Commun.* **2005**, 3343.
- (7) Fuller, L. S.; Iddon, B.; Smith, K. M. *J. Chem. Soc., Perkin Trans. 1*, **1997**, *22*, 3465.
- (8) Setsune, J. -I.; Katakami, Y.; Lizuna, N. *J. Am. Chem. Soc.* **1999**, *121*, 8957.
- (9) Rath, H.; Mallick, A.; Ghosh, T.; Kalita, A. *Chem. Commun.* **2014**, *50*, 9094.

- 1
2
3
4 (10) (a) Yoon, M.-C.; Cho, S.; Suzuki, M.; Osuka, A.; Kim, D. *J. Am. Chem. Soc.* **2009**, *131*,
5
6 7360. (b) Oh, J.; Sung, Y. M.; Kim, W.; Mori, S.; Osuka, A.; Kim, D. *Angew. Chem. Int.*
7
8 *Ed.* **2016**, *55*, 6487. (c) Shin, J.-Y.; Yoon, M.-C.; Lim, J. M.; Yoon, Z. S.; Osuka, A.
9
10 Kim, D. *Chem. Soc. Rev.* **2010**, *39*, 2751.
11
12
13
14 (11) Gaussian 09, Revision **E.01**, Frisch, M. J.; Trucks, G. W.; Schlegel, H. B.; Scuseria, G.
15
16 E.; Robb, M. A.; Cheeseman, J. R.; Scalmani, G.; Barone, V.; Mennucci, B.; Petersson,
17
18 G. A.; Nakatsuji, H.; Caricato, M.; Li, X.; Hratchian, H. P.; Izmaylov, A. F.; Bloino, J.;
19
20 Zheng, G.; Sonnenberg, J. L.; Hada, M.; Ehara, M.; Toyota, K.; Fukuda, R.; Hasegawa,
21
22 J.; Ishida, M.; Nakajima, T.; Honda, Y.; Kitao, O.; Nakai, H.; Vreven, T.; Montgomery,
23
24 J. A.; Peralta, J. E.; Ogliaro, F.; Bearpark, M.; Heyd, J. J.; Brothers, E.; Kudin, K. N.;
25
26 Staroverov, V. N.; Kobayashi, R.; Normand, J.; Raghavachari, K.; Rendell, A.; Burant, J.
27
28 C.; Iyengar, S. S.; Tomasi, J.; Cossi, M.; Rega, N.; Millam, J. M.; Klene, M.; Knox, J.
29
30 E.; Cross, J. B.; Bakken, V.; Adamo, C.; Jaramillo, J.; Gomperts, R.; Stratmann, R. E.;
31
32 Yazyev, O.; Austin, A. J.; Cammi, R.; Pomelli, C.; Ochterski, J. W.; Martin, R. L.;
33
34 Morokuma, K.; Zakrzewski, V. G.; Voth, G. A.; Salvador, P.; Dannenberg, J. J.;
35
36 Dapprich, S.; Daniels, A. D.; Farkas, Ö.; Foresman, J. B.; Ortiz, J. V.; Cioslowski, J.;
37
38 Fox, D. J. Gaussian, Inc., Wallingford CT, 2009.
39
40
41
42
43
44
45
46 (12) Kang, J. K.; Musgrave, C. B. *J. Chem. Phys.* **2001**, *115*, 11040.
47
48
49
50
51
52
53
54
55
56
57
58
59
60